PROGRESS IN PHOTOVOLTAICS: RESEARCH AND APPLICATIONS
Prog. Photovolt: Res. Appl. 2009; **17**:279–288
Published online 24 December 2008 in Wiley InterScience (www.interscience.wiley.com) DOI: 10.1002/pip.875

Research

Spectral Response and Energy Output of Concentrator Multijunction Solar Cells

Geoffrey S. Kinsey[1]*,† and Kenneth M. Edmondson[2]
[1]*Amonix Inc., 3425 Fujita St., Torrance, CA 90505, USA*
[2]*Spectrolab, Inc., 12500 Gladstone Avenue, Sylmar, CA 91342, USA*

The spectral response of concentrator multijunction solar cells has been measured over a temperature range of 25–75°C. These data are combined with reference spectra representing the AM1·5 standard as well as annual spectral irradiance at representative geographical locations. The results suggest that higher performance in the field may be obtained if multijunction cells are designed for an effective air mass higher than AM1·5. Copyright © 2008 John Wiley & Sons, Ltd.

KEY WORDS: photovoltaic cell measurements; solar energy

Received 25 August 2008; Revised 21 October 2008

INTRODUCTION

Concentrator photovoltaic (CPV) systems are attractive for utility-scale energy production due to their high energy capacity and potential for rapid scale-up. In particular, high-concentration photovoltaic (HCPV) systems employing III–V multijunction solar cells promise a low system-level cost of energy. With the demonstration of cell efficiencies over 40%,[1] development and field deployment of concentrator systems using multijunction cells has accelerated. In order to extract the maximum possible energy from a system employing III–V multijunction cells, a detailed understanding of the spectral sensitivity of the multijunction cell is required. The standard test conditions (STC) under which cells are measured consist of a temperature of 25°C and a spectrum calibrated to an AM1·5 reference such as ASTM G173-03. This method was originally developed primarily for rating fixed (non-tracking) single-junction silicon modules. However, in recent years, the market-dominant silicon cells have been bracketed on either side of their performance range by multijunction designs. Thin-film multijunctions have appeared on the low end of the cost-efficiency range[2] and III–V multijunction concentrators have appeared on the high end. Both of these multijunction technologies seek to deliver a lower levelized cost of energy via efficient partitioning of the solar spectrum.

However, the advantageous spectrum partitioning of multijunctions brings increased sensitivity to spectral variation and renders the AM1·5 spectrum less relevant in predicting overall energy output in the field.[3,4] In a HCPV system, the III–V multijunction typically operates at a temperature well above 25°C. The variability of the incident spectrum with latitude, atmospheric conditions, time of day, and day of year affects the current output of each series-connected subcell. As the understanding of the effect of these conditions grows, CPV cell and system design can be adjusted to deliver increasing annual energy output.

To this end, the spectral response of concentrator multijunction cells has been measured over the range of 25–75°C. These data were used to calculate the

* Correspondence to: Geoffrey S. Kinsey, Amonix, Inc. 3425 Fujita St., Torrance, CA 90505, USA.
† E-mail: gkinsey@amonix.com

current and power output under the AM1·5, G173-03 spectrum. Using the NREL SMARTS model,[5,6] annual spectral irradiance for several reference locations was generated to predict annual current and energy output. Comparisons with the results under the AM1·5 spectrum point to the potential benefits of designing the cells for operation under a higher effective air mass.

III–V MULTIJUNCTION DESIGN

The high efficiency of the present III–V multijunction cell is obtained by employing three subcells to partition the incident solar spectrum and produce a higher voltage and lower current than is obtained by, for example, a single-junction silicon cell. The partitioning of the solar spectrum among three subcells results in an increased sensitivity to changes in the spectral content. The three-junction structure consists of a GaInP top subcell and a low-indium Ga(In)As middle subcell lattice-matched to the Ge bottom subcell. Under the AM1·5 spectrum, the band gaps of GaInP and the Ga(In)As are such that more than a third of the available photons pass through them and excess current is generated in the bottom, Ge, subcell. The top and middle subcells are therefore the limiters of the overall cell current.

For optimum performance under the AM1·5, direct (G173-03) reference spectrum, the top and middle subcells are designed to produce equal currents under this specific spectrum. When the currents from these two subcells are equal, the ''current match'' condition balances the two subcell currents and prevents either from limiting the three-junction stack. A deviation in the spectrum away from AM1·5 will cause one of the subcells to become the current limiter. A figure of merit in three-junction cell design is therefore the ratio of the current densities of the top and middle subcells. The ratio of the top to middle subcell current density will be referred to below as ''J_T/J_M''. Under a given spectrum, the highest current output for a three-junction cell is obtained at current match, with J_T/J_M equal to one.

For a cell designed to deliver this current-matched condition under the AM1·5 spectrum, a change in spectrum corresponding to a higher air mass, for example, will provide less short-wavelength radiation to be absorbed in the top subcell, starving it for current and resulting in a J_T/J_M less than one. Conversely, a lower effective air mass produces a J_T/J_M greater than one. For the present multijunction structure, it is generally easier to design for a lower J_T/J_M than a higher J_T/J_M. To produce a lower J_T/J_M, the top subcell may be thinned to allow additional light to reach the middle subcell. Down-conversion mechanisms such as radiative coupling may also augment the middle subcell current.[7] Complementary processes to augment top subcell current are less viable, although it is possible to re-tune the anti-reflective coating to favor the top subcell.

Temperature variation presents another variable in optimization of the cell design.[8] STC dictate cell measurement at 25°C, whereas a cell integrated with a high-concentration optical system typically operates in the 40–80°C range. A rise in temperature decreases the band gaps of the various subcell materials and shifts the wavelength range that is absorbed by each subcell. This shifts the J_T/J_M with respect to that measured at the standard temperature of 25°C.

SPECTRAL RESPONSE MEASUREMENT

The spectral response of concentrator multijunction solar cells was measured as a function of temperature. The Spectrolab multijunction solar cell devices under test were the C1MJ (''Concentrator, first-generation Multijunction'') and a prototype C2MJ. The C1MJ cell has been in production since 2006; C1MJ cells have passed a qualification program and are now installed in several CPV systems around the world. Several design variations were evaluated for the C2MJ cell. The particular ''prototype C2MJ'' cell evaluated in this work has a top subcell with a wider band gap, resulting in a higher voltage output than the C1MJ. This is the same prototype C2MJ structure evaluated in Reference 9. However, this prototype did not become the final C2MJ design that was implemented in production in 2008. The term ''prototype C2MJ'' is retained for consistency with Reference 9.

Both cell designs have an anti-reflective coating that is optimized for mating with a glass optical component assumed to have a refractive index of 1·43. The cells in this study were measured bare (without a glass optical component); the results presented below include a reflectance correction factor applied to the raw data to represent performance expected under an index-matched optical component such as a coverglass, prism, or conformal coating.

The spectral response measurement technique is similar to that published elsewhere.[10,11] A tungsten-halogen light source and high-resolution monochromator were used to deliver low-intensity illumination

DOI: 10.1002/pip

at 5 nm wavelength increments to a small area within the aperture area of typical 1 cm^2 concentrator cells. To select for a particular subcell under test, the incident beam was chopped and the resulting subcell current output was detected using a lock-in amplifier. To avoid having the current limited by the two subcells not under test, steady-state, filtered light bias was applied to generate excess DC current in those subcells. A DC electrical bias was also applied to maintain the subcell under test close to its short-circuit current condition.

The cells were vacuum mounted on a brass stage that was water cooled/heated to control the cell temperature. The temperature was monitored via a thermocouple mounted adjacent to the cell under test. For measurement of the top and middle subcells, the system was calibrated using a silicon reference standard. Subcells in fully active three-junction structures were evaluated. For measurement of the germanium bottom subcell, a separate measurement was conducted via calibration using a germanium reference standard. The devices under test were then C1MJ germanium isotype cells. A germanium isotype cell consists of the active germanium (bottom) subcell beneath inactive top and middle subcell materials formed without p-n junctions.

The spectral response of the subcells were measured at 25, 45, 65, and 75°C. Results for the top and middle subcells for C1MJ and the prototype C2MJ are shown in Figures 1 and 2, respectively. Data shown is the mean for five cells measured for each design. Results for a single C1MJ germanium subcell isotype are shown in Figure 3. Due to their proximity to the 75°C data, the 65°C results are omitted from the figures to improve clarity. The contour of the G173-03 spectrum is included in the background, for reference. As cell temperature rises, the band gap of each subcell is lowered, causing the spectral response to shift towards longer wavelengths. This shifts its alignment with respect to the solar spectrum. For the top subcell, this means an increase in the available photons. At 75°C, the middle subcell approaches a falloff in available photons near 900 nm as a result of the water absorption band. As a result of these combined effects, J_T/J_M is expected to increase with temperature.

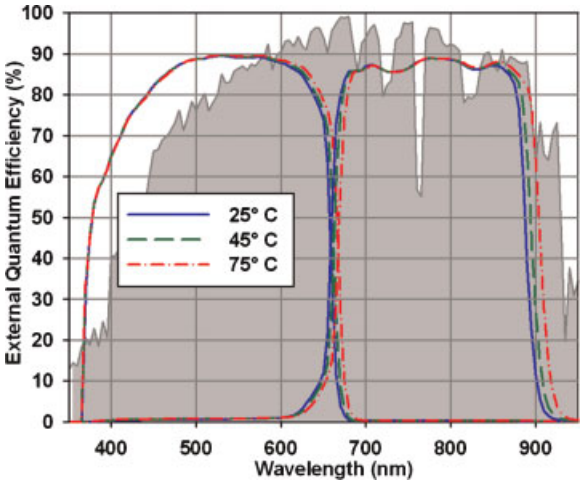

Figure 2. Spectral response of top and middle subcells of a prototype C2MJ multijunction at 25, 45, and 75°C

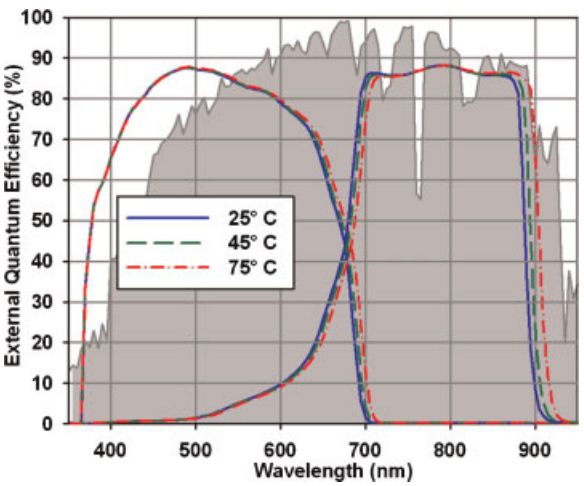

Figure 1. Spectral response of top and middle subcells of the C1MJ multijunction at 25, 45, and 75°C

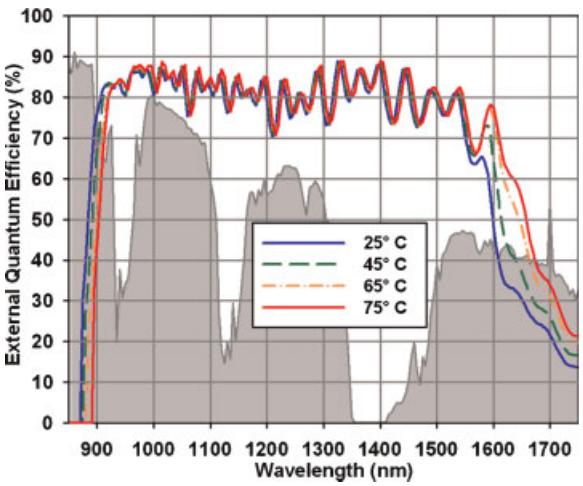

Figure 3. Spectral response of a C1MJ bottom subcell isotype at 25, 45, 65, and 75°C

DOI: 10.1002/pip

BAND GAP TEMPERATURE DEPENDENCE

The temperature dependence of each band gap and its resulting derivative, can be expressed as[12]

$$E_g(T) = E_g(0) - \frac{\alpha T^2}{T+\beta} \quad (1)$$

$$\frac{\partial E_g}{\partial T} = -\frac{2\alpha T}{T+\beta} + \frac{\alpha T^2}{(T+\beta)^2} \quad (2)$$

Empirical values for α and β are available for GaInP, GaAs, and Ge material.[13–15] Using the GaAs data set to represent the Ga(In)As material, substitution into Equation (1) yields the predicted change in band gap with temperature indicated by the lines in Figure 4.

The data points were obtained from the spectral response data. For direct band gap semiconductors, the quantum efficiency at the band edge is proportional to the square root of the band gap.[16] Accordingly, the band gap can be extracted from the quantum efficiency data by determining the x-axis intercept of a linear fit to the square of the quantum efficiency plotted against photon energy. For indirect band gap materials such as germanium, this approach is less accurate, as can be seen in Figure 4 in the deviation of that data set from the prediction.

The change in band gap with temperature indicated by Equation (2) is higher for GaInP than for GaAs. For example, evaluation of Equation (2) at 65°C yields a value of $5{\cdot}3 \times 10^{-4}$ eV/°C for GaInP and $4{\cdot}6 \times 10^{-4}$ eV/°C for GaAs. As temperature is increased, the absorption band energy of the top subcell will shift more than that of the middle subcell, causing a rise in J_T/J_M with temperature. This augments a rise in J_T/J_M due to the re-alignment with respect to the bands in the solar spectrum discussed above. The shift to higher J_T/J_M with temperature is advantageous given that higher J_T/J_M is generally more difficult to achieve. It should be noted that, in Figures 1 and 2, the shift in the Ga(In)As band edge appears larger than that of the GaInP band edge. This is due to the use of wavelength for the x-axis, which is proportional to the inverse of photon energy.

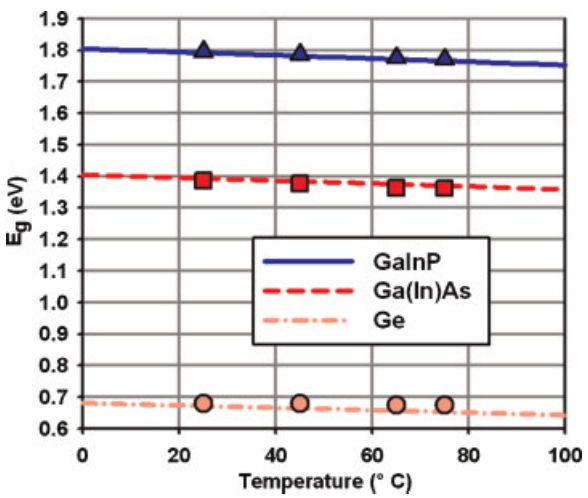

Figure 4. Temperature dependence of the band gaps of C1MJ subcells

CURRENT AND POWER UNDER THE AM1·5 SPECTRUM

Using the spectral response data above, it is possible to predict the output current density and power of the multijunction solar cells under the AM1·5 reference spectrum. The irradiance of the AM1·5, G173-03 (direct) reference spectrum is used to calculate the number of photons available in the wavelength bands of the spectral response data. Assuming each photon could create an electron-hole pair, an equivalent ''available'' current density in each 5 nm interval is then calculated. Convolution with the cell quantum efficiency yields the expected short-circuit current generated in each subcell under this spectrum. For the purposes of comparison, the quantum efficiency data of all subcells was normalized to a maximum magnitude of 89%.

The results are indicated in Tables I and II. For both cell designs, the J_T/J_M target was 1·0 at a temperature of 25°C. For the particular cells tested, the actual J_T/J_M was less than the target, indicating a top subcell that was under-producing current with respect to the middle subcell. J_T/J_M of the prototype C2MJ cells was particularly low. The higher band gap of the prototype C2MJ top subcell makes a J_T/J_M of 1·0 harder to consistently achieve. Both cell designs showed the expected increase in J_T/J_M with temperature.

Under the AM1·5 spectrum, the excess current available in the bottom subcell remains above 32% for both cell designs at all temperatures. This excess current plays a role in both heating the cell and in maintaining a high fill factor for the multijunction. Under conditions of reduced excess bottom subcell current, the low fill factor of the bottom subcell will

DOI: 10.1002/pip

Table I. C1MJ cell under the G173-03 spectrum

C1MJ	25°C	45°C	65°C	75°C	d/dT (/°C)
Top subcell current density (mA/cm^2)	12·6	12·8	12·9	13·0	0·07%
Middle subcell current density (mA/cm^2)	12·7	12·9	13·0	13·1	0·06%
Bottom subcell current density (mA/cm^2)	19·0	19·2	19·3	19·3	0·03%
Top/middle J ratio	0·993	0·993	0·996	0·998	0·01%
Excess bottom subcell current	33·7%	33·3%	32·9%	32·4%	−0·07%
V_{oc} (V)	3·150	3·064	2·979	2·936	−0·14%
Fill factor	0·850	0·840	0·830	0·825	−0·06%
Power density (W/cm^2)	18·74	18·25	17·77	17·52	−0·13%
Efficiency (50 W/cm^2)	37·5%	36·5%	35·5%	35·0%	−0·13%

become evident in the multijunction current-voltage characteristic. This is discussed in the appendix.

In order to estimate instantaneous power output, the cell current data were combined with temperature-dependent voltage and fill factor data measured previously. As part of the analysis in Reference 9, temperature-dependent open-circuit voltage and fill factor values were measured under 555× concentration. Measurements were made using a Spectrolab High-Intensity Pulsed Solar Simulator (HIPSS). A concentration of 1× is defined here as 0·09 W/cm^2, AM1·5 ASTM G173-03 standard spectrum. A concentration of 555× therefore corresponds to 50 W/cm^2 incident power. Representative values of voltage and fill factor for both cell designs are included in Tables I and II below. The expected current output at 555× concentration was calculated by assuming that the multijunction cells, designed for operation at 555×, operate at concentration levels where the current is linear with concentration.[9,11,17] The 1× current densities may therefore be scaled accordingly. The last column of Tables I and II indicates the temperature dependence of each parameter, expressed as a percentage of the value measured at 25°C. The current temperature coefficients are consistent with those found in Reference 10.

For both designs, the modest increase in current with temperature is more than offset by the decrease in voltage, so power density and efficiency decline accordingly. Due to the higher current mismatch in the prototype C2MJ cells measured, they produce a lower power than the C1MJ cells at 25°C. As temperatures rise, however, the prototype C2MJ cells provide increasingly higher power with respect to the C1MJ cells. Measurement under STC therefore fails to predict the optimum design at higher (operating) temperatures.

PREDICTION OF ANNUAL CURRENT OUTPUT

Analysis of the multijunction cell output under AM1·5 is a first step in understanding how much energy a multijunction will produce in the field. In order to estimate the annual energy output, additional spectral conditions must be examined. The NREL SMARTS model[5,6] provides a convenient method to generate spectral irradiance data at various hypothetical geographic locations. For a given latitude and elevation, the model may be used to generate the available direct normal spectral irradiance ([W/m^2 nm] at 5 nm intervals) throughout a day and year. Convolution

Table II. Prototype C2MJ cell under the G173-03 spectrum

Prototype C2MJ	25°C	45°C	65°C	75°C	d/dT (/°C)
Top subcell current density (mA/cm^2)	12·2	12·4	12·6	12·7	0·09%
Middle subcell current density (mA/cm^2)	12·7	12·9	13·0	13·0	0·04%
Bottom subcell current density (mA/cm^2)	19·0	19·2	19·3	19·3	0·03%
Top/middle J ratio	0·957	0·963	0·973	0·977	0·04%
Excess bottom subcell current density	35·9%	35·4%	34·7%	34·1%	−0·10%
V_{oc} (V)	3·210	3·124	3·038	2·995	−0·13%
Fill factor	0·860	0·851	0·842	0·838	−0·05%
Power density (W/cm^2)	18·66	18·27	17·89	17·68	−0·10%
Efficiency (50 W/cm^2)	37·3%	36·5%	35·8%	35·4%	−0·10%

DOI: 10.1002/pip

with the cell spectral response yields the current generated at a given date and time. This provides a means for estimating the cell annual energy output.

Output spectra were generated in the wavelength range of 350–1800 nm for three locations. These were (in order of decreasing geographic latitude): Madrid (Spain), Phoenix (USA), and Alice Springs (Australia). Spectral irradiance output was generated in 2 h intervals during daytime for one day in each month of the year. For the case of Phoenix, this resulted in 72 data sets used to form the contour plots that follow. For a location at lower latitude, more daytime hours would produce additional data points. The US Standard Atmosphere for 1976 was used as the reference atmosphere. A low air turbidity value of 0·084 (the default) was used, clear skies were assumed, and no loss factor due to the concentrating optics was applied. In general, concentrating optics tend to have lower optical transmission in the wavelength range of the top subcell, delivering a spectrum consistent with a higher effective air mass. The results that follow therefore represent something of an upper bound for actual energy output in CPV systems in the field. As additional detailed spectral irradiance data are collected from the field, refinements to the results below will be possible.[18] Nevertheless, trends in these results provide insight for future design directions.

The SMARTS spectral irradiance output for Phoenix, USA is shown in Figure 5. For comparison, outdoor measurements from the NREL Typical Meteorological

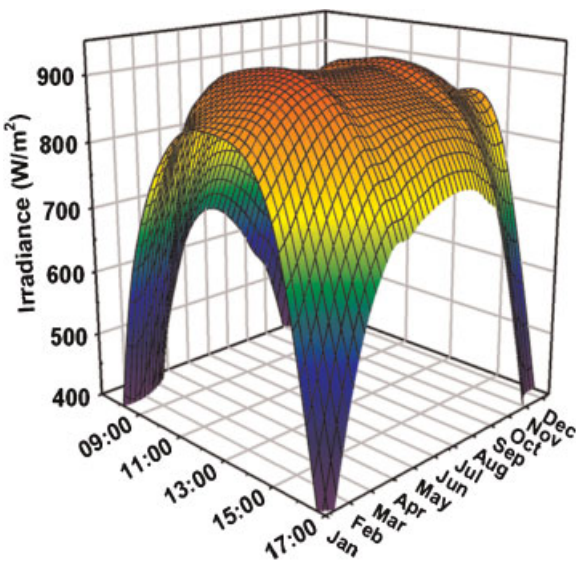

Figure 5. SMARTS model direct normal irradiance for Phoenix, USA in the wavelength range of 350–1800 nm

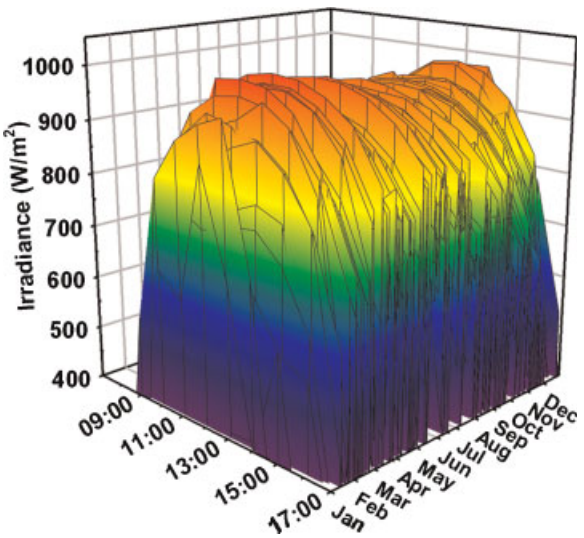

Figure 6. Typical Meteorological Year 2 (1961–1990) direct normal irradiance for Phoenix, USA

Year 2 (TMY2) direct normal irradiance data for Phoenix is shown in Figure 6.[19] The TMY2 data set, which includes the influence of cloud cover and local weather variations, is comparable in shape to the output generated by SMARTS. The maximum irradiance seen in the TMY2 data are slightly higher since the SMARTS modeled output was limited to the range of wavelengths absorbed by a multijunction.

The projected annual current output of the multijunction cell is obtained by convolution of the modeled spectral irradiance output from SMARTS with the cell spectral response and subsequent summation of the 5 nm wavelength elements. As an example, the conditions at a cell temperature of 65°C in Phoenix are shown in the contour plots below. It should be noted that the cell temperature assumed here is based on the cell spectral response measurements and is therefore independent of the various air temperatures implicit in the SMARTS model outputs. Under these conditions, J_T/J_M (Figure 7) is slightly greater than one in the summer months during the middle of the day. Since the resulting excess current in the top subcell does not contribute to current in the overall stack, the multijunction produces more current in the spring and fall, when J_T/J_M is closest to one. During the spring and fall in Phoenix, there is a slight increase in solar irradiance (Figures 5 and 6): the compound effect of these two factors is a pronounced increase in overall multijunction current density during the spring and fall (Figure 8).

DOI: 10.1002/pip

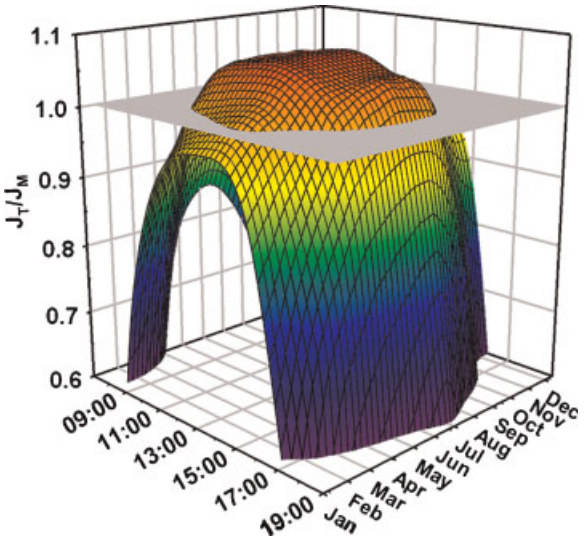

Figure 7. Top/middle subcell current density ratio for a C1MJ cell at a cell temperature of 65°C in Phoenix. The current-match condition ($J_T/J_M = 1$) is indicated in gray. For points below this plane, the top subcell limits the overall current

In order to get a sense of the potential for improvement in J_T/J_M in future cell designs, a ''weighted annual J_T/J_M'' was calculated. Each J_T/J_M at a given data point was weighted by the total current available to the top and middle cell at that point. The sum of these values, divided by the total annual current, provides the weighted annual J_T/J_M indicated in Figures 10 and 11. The results are discussed in relation to energy output in the section that follows.

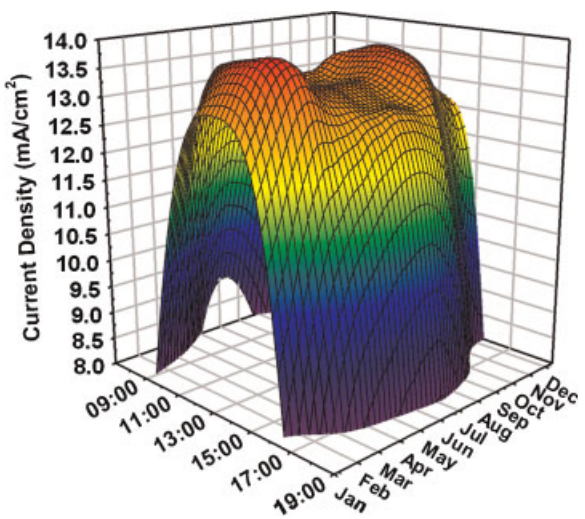

Figure 8. Short-circuit current density for a C1MJ cell at 1× and a cell temperature of 65°C in Phoenix

To determine the typical amount of excess bottom subcell current available, a weighted annual excess bottom current density ratio was calculated, using the current available to all three subcells as the weighting factor. The weighted annual excess bottom subcell current ratio ranged from a low of 39% (for a C1MJ cell at 75° in Alice Springs) to 41% (for a C2MJ cell at 25° in Alice Springs). The higher excess current with respect to AM1·5 is consistent with the generally lower J_T/J_M with respect to AM1·5. The effect of the higher annual excess bottom subcell current on fill factor is discussed in the appendix.

PREDICTION OF ANNUAL ENERGY OUTPUT

Following a process similar to that used above in evaluating the cell power output under the AM1·5 spectrum, cell energy output under the variable field spectral conditions can be predicted. In order to account for variations in intensity, intensity weighting functions were applied to the cell voltage for each data set. As shown in Reference 9, the open-circuit voltage has a logarithmic dependence on intensity

$$V_{oc} = \frac{nkT}{q\log(e)}\log(X) + V_{oc,X=1} \text{ for } e^{\frac{qV_{oc,X=1}}{nkT}} >> 1, \frac{1}{X} \quad (3)$$

Based on the measurements in Reference 9, an ideality factor for the multijunction diode of 3·4 was assumed in Equation (3) to obtain the appropriate intensity corrections to the measured open-circuit voltage at 50 W/cm^2. The fill factor was corrected for temperature, but not for intensity or spectral variation. In order to simplify the analysis, fill factor variations are largely neglected in this study. However, variations in fill factor can have a significant impact on performance. For example, it has been observed that a rise in fill factor due to current mismatch can partially offset the decrease in current that results.[3] The effect of intensity variation on fill factor will depend on the particular metal coverage ratio applied to a given cell. The potential impact of spectral variation on the fill factor is treated in the appendix.

Based on the assumptions above, the resulting instantaneous power output is shown in Figure 9. The value at each data point was summed to obtain an

DOI: 10.1002/pip

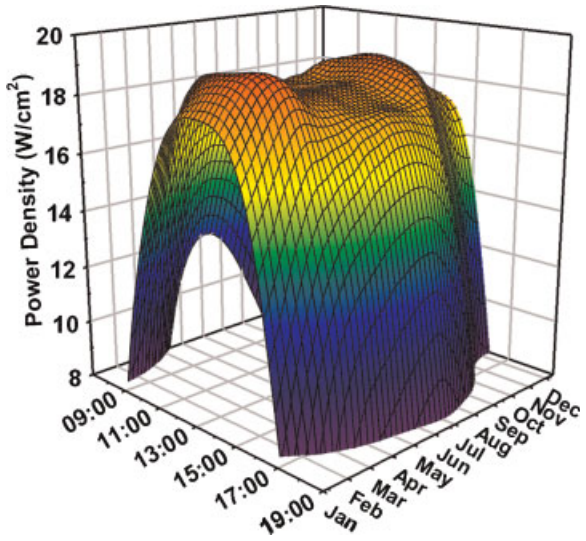

Figure 9. Projected power output for a C1MJ cell at 500× and a cell temperature of 65°C in Phoenix

estimate of the annual energy output at 555× optical concentration for a 1 cm^2 cell.

Weighted annual J_T/J_M and energy output at the three locations, in order of decreasing latitude, for C1MJ and prototype C2MJ cells are shown in Figures 10 and 11, respectively. As might be expected, J_T/J_M and the energy output increase with decreasing latitude for both cell designs. Despite consistently lower weighted annual J_T/J_M, the prototype C2MJ cells provide higher annual energy output under all conditions. Though testing at 25°C under AM1·5 would have suggested otherwise, the advantage of higher cell voltage outweighs the decrease in current due to current mismatch.

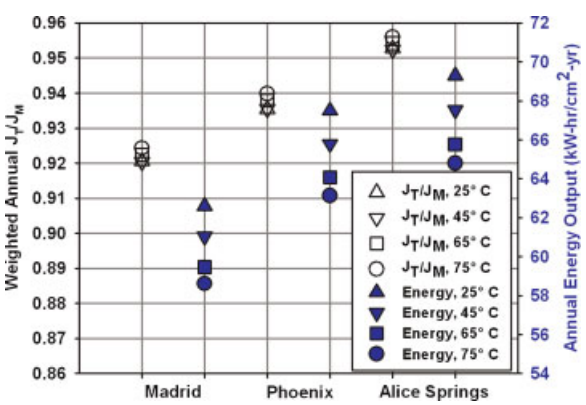

Figure 10. Predicted annual output of C1MJ cells at several locations

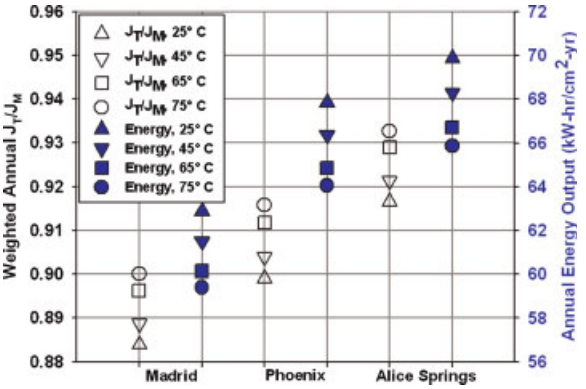

Figure 11. Predicted annual output of prototype C2MJ cells at several locations

Annual energy output ranges from a low of 59 kW hr/cm^2 yr for a C1MJ at 75°C in Madrid to a high of 70 kW hr/cm^2 yr for a prototype C2MJ at 25°C in Alice Springs. Assuming 555× concentration over the wavelength range of 350–1800 nm, the corresponding annual insolation values predicted by SMARTS for Madrid, Phoenix, and Alice Springs are 173, 183, and 187 kW hr/cm^2 yr, respectively. The annual mean cell conversion efficiencies therefore range from a low of 34% for C1MJs at 75°C in Madrid to a high of 37% for prototype C2MJs at 25°C in Alice Springs.

The weighted annual J_T/J_M of both designs is markedly lower than that under AM1·5 (G173-03). This suggests that, over the course of a year, significant excess current is generated in the middle subcell, only to be lost in carrier recombination due to top subcell current limitations. One of the principal appeals of HCPV systems for utility-scale applications is that the high cell efficiencies serve to justify the use of expensive, precision dual-axis tracking components. This tracking, in turn, provides more consistent power output throughout the day compared to fixed or single-axis-tracking systems. This consistency in power output is a signature advantage for large-scale utility systems intended to provide a significant portion of the power in an electrical grid. Sub-optimal current matching substantially undermines this potential.

Cell structures designed for a higher effective air mass would produce more consistent and higher overall annual energy output. This is particularly true for the higher-band-gap prototype C2MJ design, for which J_T/J_M is only approximately 0·9 at 65°C in Phoenix. This J_T/J_M might be increased by 10%, to approximately 1·0, by appropriate re-optimization of the cell design. Assuming any increase in top subcell

DOI: 10.1002/pip

current comes at the expense of the middle subcell current, a J_T/J_M of 1·0 would still yield an increase in annual current (and energy output) of 5%. This might be achieved by thickening of the top subcell, for example, or by re-tuning the anti-reflective coating.

The results above are an indication that a cell optimized for operation at AM1·5 may not be well-optimized for operation in the field. Rather, aiming for a higher effective air mass appears to be the preferred design direction. Concentrating optics, whether refractive or reflective, tend to have their lowest transmission in the wavelength range of the top subcell. If these effects are considered, the advantage of re-optimization of the cell structure for higher effective air mass is compounded.

CONCLUSION

The spectral response of multijunction solar cells has been measured over the temperature range of 25–75°C. These data have been used to predict cell performance under the AM1·5 reference spectrum and under annual spectra representing several field locations. Comparison of cell performance in field conditions with those at AM1·5 and 25°C suggest that significant improvements in annual energy output may be realized by designing multijunctions for operation at elevated temperature and an effective air mass higher than AM1·5.

Acknowledgements

The authors thank Juan Valles, Randy Brandt, Takahiro Isshiki, Dmitri Krut, Peichen Pien, Peter Hebert, Richard King, Mark Takahashi, Kent Barbour, Don Aldrich, and the entire multijunction solar cell team at Spectrolab. This work was supported in part by the Department of Energy's Solar America Initiative and by Spectrolab.

REFERENCES

1. King RR, Law DC, Edmondson KM, Fetzer CM, Kinsey GS, Yoon H, Sherif RA, Karam NH. 40%-efficient metamorphic GaInP/GaInAs/Ge multijunction solar cells. *Applied Physics Letters* 2007; **90**: 183516.
2. Yoshimi M, Sasaki T, Sawada T, Suezaki T, Meguro T, Matsuda T, Santo K, Wadano K, Ichikawa M, Nakajima A, Yamamoto K. High efficiency thin film silicon hybrid solar cell module on 1 m^2-class large area substrate. *Proceedings of 3rd World Conference on Photovoltaic Energy Conversion*, Vol. 1, May 2003; 1566–1569.
3. Faine P, Kurtz SR, Riordan C, Olson JM. The influence of spectral solar irradiance variations on the performance of selected single-junction and multijunction solar cells. *Solar Cells* 1991; **31**: 259–278.
4. Keith Emery, Daryl Myers, Sarah Kurtz. What is the appropriate reference spectrum for characterizing concentrator cells? *Proceedings of 29th IEEE Photovoltaic Specialists Conference,* 2002; 840–843.
5. Gueymard C. Parameterized transmittance model for direct beam and circumsolar spectral irradiance. *Solar Energy* 2001; **71**(5); 325–346.
6. Gueymard C. SMARTS, a. simple model of the atmospheric radiative transfer of sunshine: algorithms and performance assessment. *Professional Paper FSEC-PF-270-95*, 2005.
7. Yoon H, King RR, Kinsey GS, Kurtz S, Krut DD. Radiative coupling effects in GaInP/GaAs/Ge multijunction solar cells. *Proceedings of 3rd World Conference on Photovoltaic Energy Conversion*, Vol. 1, May 2003; 745–748.
8. Wanlass MW, Emery KA, Gessert TA, Horner GS, Osterwald CR, Coutts TJ. Practical considerations in tandem cell modelling. *Solar Cells* 1989; **27**: 191–204.
9. Kinsey GS, Hebert P, Barbour KE, Krut DD, Cotal HL, Sherif RA. Concentrator multijunction solar cells. *Progress in Photovoltaics: Research and Applications* 2008; **16**(6): 503–508.
10. Aiken D, Stan M, Murray C, Sharps P, Hills J, Clevenger B. Temperature dependent spectral response measurements for III–V multi-junction solar cells. *Proceedings of the 29th IEEE PVSC* 2002; 828–831.
11. Emery K, Meusel M, Beckert R, Dimroth F, Bett A, Warta W. Procedures for evaluating multijunction concentrators. *Proceedings of the 28th IEEE PVSC* 2000; 1126–1130.
12. Varshni YP. Temperature dependence of the energy gap in semiconductors. *Physica* 1967; **34**(1): 149–154.
13. Swaminathan V, Macrander AT. *Materials Aspects of GaAs and InP Based Structures*. Prentice-Hall: Englewood Cliffs, NJ, 1991; 18.
14. Van Zeghbroeck BJ. *Principles of Semiconductor Devices*, 1997; Available at: http://ece-www.colorado.edu/∼bart/book/eband5.htm
15. Fan JCC. Theoretical temperature dependence of solar cell parameters. *Solar Cells* 1986; **17**: 309–315.
16. Smestad GP. *Optoelectronics of Solar Cells*, Vol. 48. SPIE Press: Bellingham, WA, 2002; 23–24.
17. Stryi-Hipp G, Schoenecker A, Schitterer K, Bucher K, Heidler K. Precision spectral response and I–V characterization of concentrator cells. *Proceedings of the 23rd IEEE PVSC* 1993; 303–308.
18. Ekins-Daukes NJ. Evaluation of InGaP/InGaAs/Ge concentrator system annual yield and comparison to estimates based on reference spectra. *Proceedings of the 33rd IEEE PVSC*, 2008.

DOI: 10.1002/pip

19. National Solar Radiation Database. Available at: http://rredc.nrel.gov/solar/old_data/nsrdb/tmy2/
20. Geisz JF, Kurtz S, Wanlass MW, Ward JS, Duda A, Friedman DJ, Olson JM, McMahon WE, Moriarty TE, Kiehl JT. High-efficiency GaInP/GaAs/InGaAs triple-junction solar cells grown inverted with a metamorphic bottom junction. *Applied Physics Letters* 2007; **91**: 023502.
21. McMahon WE, Emery KE, Friedman DJ, Ottoson L, Young MS, Ward JS, Kramer CM, Duda A, Sarah Kurtz. Fill factor as a probe of current-matching for $GaInP_2$/GaAs tandem cells in a concentrator system during outdoor operation. *Progress in Photovoltaics: Research and Applications* 2008; **16**: 213–224.

APPENDIX: CURRENT ALLOCATION AND FILL FACTOR

Due to its narrow band gap (0·67 eV), the present bottom subcell of the III–V multijunction cell has a significantly lower fill factor than that of the other two subcells. The relative importance of this depends on the amount of excess current available to be generated by the bottom subcell. Under the AM0 and AM1·5 spectra, there is enough excess current allocated to the bottom subcell to avoid a significant impact on the overall fill factor of the multijunction stack. With sufficient excess current generated in the bottom subcell, the current match condition is obtained well to the right of the knee in the bottom subcell current-voltage characteristic: changes in current do not result in significant changes in subcell voltage.

The excess current available is sensitive to both temperature and spectral conditions. Changes in the cell design can also alter the ratio. Future high-efficiency cell designs, such as metamorphic three-junctions[1,20] and some four-junction designs, increase cell efficiency by increasing the absorption in other subcells or by increasing the bottom subcell band gap, effectively reducing the excess current allocated to the bottom subcell. Techniques to reduce cell absorptance (to decrease cell temperature) will also decrease the excess current available. As the excess current decreases, the low fill factor of the bottom subcell becomes increasingly evident in the fill factor of the full multijunction.[21] This could partially offset the anticipated advantages.

To illustrate this effect, measurements at 555× were used to generate subcell current-voltage characteristics of a top-middle two-junction cell and a bottom subcell isotype (Figure 12). The two-junction cell has a fill factor of 0·845. A family of six curves representing 5% relative decrements in bottom subcell current was used to simulate decrease of current in the bottom subcell. The highest bottom subcell current shown has 42% excess current with respect to the two-junction cell and a fill factor of 0·62.

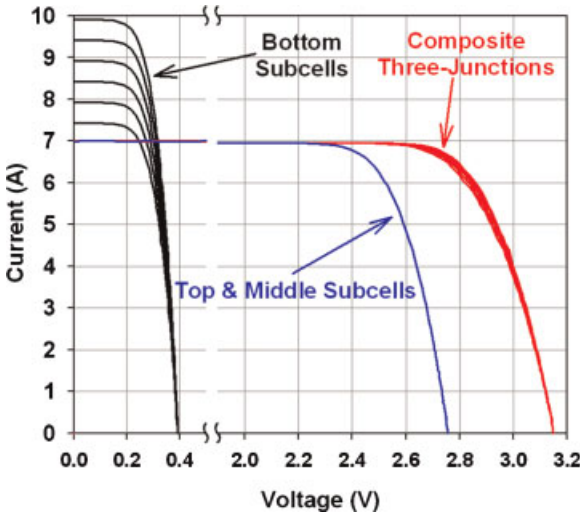

Figure 12. Effect of excess bottom subcell current on the current-voltage characteristic

Three-junction composite current-voltage characteristics were generated by combining the two-junction curve with each of the bottom subcell curves by summing the subcell voltages at points where the currents were closely matched. The resulting decrease in fill factor with decrease in excess current is evident in the composite three-junction curves in Figure 12 and in Table III. Based on these results, a modest increase in fill factor of 0·003 might be expected in moving from an excess current of approximately 34% under AM1·5 up to the 40% range found for the geographic locations examined above. This provides confidence that future designs that require a reduction in excess bottom subcell current have some design margin with respect to potential loss in fill factor.

Table III. Impact of bottom subcell on fill factor

Excess bottom subcell current	Three-junction fill factor
42%	0·838
35%	0·835
28%	0·833
20%	0·831
13%	0·827
6%	0·820

DOI: 10.1002/pip